# Supporting Information

## Löhr et al. 10.1073/pnas.0910225106

### SI Materials and Methods

**Plasmid Construction.** The 3′ end of the *bcd* cDNA was amplified by PCR with an internal 5′ primer (bcd_orfp: cagcacaaggaccagtcc) and a 3′ primer (bcd_Xba3′p: tatctagaggctaattgaagcagtaggc) that added an XbaI site downstream of the internal stop codon and fidelity was verified by sequencing. The 5′ region of the *bcd* cDNA was released from pBluescript by NotI/BglII digest, both fragments were cloned into the NotI/XbaI site of the UASp vector (8). The resulting vector UASp-*bcdΔ3′UTR* was injected into $w^{1118}$ flies using standard techniques.

A fragment containing the *attB* sequence was cloned into the pCaSpeR-hs43-*lacZ* using EcoRI and NotI, creating the vector *attB*N-hs43-*lacZ*. The following oligonucleotides, containing 5′ NotI and 3′ XbaI overhangs were used for cloning into the p*attB*N-hs43-*lacZ* vector:

bcd3T (7): ggccgcaggttc**taatcc**cggtc**taatcc**ctcgagtc**taatcc**catgagtcgacgt; Bcd binding sites are in bold.

bcd3T_1torREu: ggccgctgctcaatgaaaggttc**taatcc**cggtc**taatcc**ctcgagtc**taatcc**catgagtcgacgt; the torRE (9) is underlined; Bcd binding sites are in bold.

bcd3T_2torRE: ggccgctgctcaatgaaaggttc**taatcc**cggtc**taatcc**ctcgagtc**taatcc**catgagtcgacgtgctcaatgaat; the torREs are underlined; the Bcd binding sites are in bold.

The annealed and phosphorylated oligonucleotides were cloned into the NotI and SpeI sites of *attB*N-hs43-*lacZ*; the resulting vectors were named bcd3t-*lacZ*, bcd3T_1torREu-*lacZ*, and bcd3T_2torRE-*lacZ*. Primers and oligonucleotides were produced by MWG.

**Fly Crosses.** To ectopically express unlocalized Bcd in the female germline, females homozygous for V3 were crossed to males homozygous for UASp-*bcdΔ3′UTR*. Embryos from V3/*X*; UASp-*bcdΔ3′UTR*/*II* females crossed to $w^{1118}$ males were analyzed. For ubiquitous Bcd expression in $bcd^{E1}$ embryos V3/V3; $bcd^{E1}$/*TM3* virgins were crossed to males homozygous for UASp-*bcdΔ3′UTR;* $bcd^{E1}$. Embryos from V3/*X*; UASp-*bcdΔ3′UTR*/*II*; $bcd^{E1}$/$bcd^{E1}$ females crossed to $w^{1118}$ males were analyzed. For ubiquitous Bcd in $tor^{PM}$ embryos, V3/V3; $tor^{PM}$/*CyO* virgins were crossed with males homozygous for $tor^{PM}$; UASp-*bcdΔ3′UTR*. Embryos laid by V3/*X*; $tor^{PM}$/$tor^{PM}$; UASp-*bcdΔ3′UTR*/*III* females crossed to $w^{1118}$ males were evaluated. For ubiquitous Bcd in $cic^{1}$ embryos, V3/V3; $cic^{1}$/*TM3* virgins were crossed to males homozygous for UASp-*bcdΔ3′UTR*; $cic^{1}$. Embryos from V3/*X*; UASp-*bcdΔ3′UTR*/*II*; $cic^{1}$/$cic^{1}$ females crossed to $w^{1118}$ males were analyzed. For ubiquitous Bcd in *tor, cic* double mutant embryos V3/V3; $tor^{PM}$/*CyO*; $cic^{1}$/*TM3* virgins were crossed to males homozygous for $tor^{WK}$, UASp-*bcdΔ3′UTR;* $cic^{1}$. Embryos from V3/*X*; $tor^{PM}$/$tor^{WK}$, UASp-*bcdΔ3′UTR*; $cic^{1}$/$cic^{1}$ females crossed to $w^{1118}$ males were evaluated. To evaluate the effects of unlocalized Bcd on the cnc_(+5) and the gt_(−6) enhancer modules (3), embryos from V3/*X*; UASp-bcdΔ3′UTR/*II* females crossed to males homozygous for cnc_(+5)-*lacZ* or gt_(−6)-*lacZ* were analyzed.

**DIG-Labeled *in situ* Hybridization Detected by Alkaline-Phosphatase.** Embryos were collected for 3 h and *in situ* hybridizations using the appropriate DIG labeled anti-sense probes were conducted using standard methods. DIG was detected using sheep anti-DIG antibodies coupled to alkaline phosphatase (Roche) and visualized using NBT/BCIP solution (Roche). Embryos were dehydrated, mounted in Canada Balsam (Sigma), and cross-sections through the embryo were photographed using the Nomarski optics of an Axiophot microscope (Zeiss) with a digital camera (Kontron Elektronik) and the appropriate software.

**Fluorescent Double *in situs* and Immunohistochemistry.** DIG and FITC-labeled RNA probes against *tll* and *cnc* mRNA, respectively, were made using standard methods. Both probes were hybridized to embryos at the same time at 57 °C overnight. The FITC-labeled probe was detected with mouse anti-FITC antibodies (Roche) and biotinylated anti-mouse antibodies from goat (Jackson ImmunoResearch). For signal amplification, embryos were incubated with ABC reagent (Vector Laboratories) for 30 min, followed by a 5-min incubation with TSA Fluorescein reagent (Perkin–Elmer) diluted 1:50. HRP was deactivated by a 10-min incubation at 70 °C and free biotin was blocked using the blocking kit (Vector Laboratories). The DIG-labeled probe was detected with sheep anti-DIG antibodies (Roche) and biotinylated anti-sheep antibodies from donkey (Jackson ImmunoResearch). For signal amplification, embryos were incubated with ABC reagents for 30 min, followed by a 5-min incubation with TSA Cy5 reagents (Perkin–Elmer) diluted 1:50. Anti-Gt antibodies from rabbit (10) were diluted 1:400 and detected with Alexa 568 anti-rabbit antibodies from donkey (Invitrogen). Embryos were mounted in Vectashield with DAPI (Vector Laboratories) and visualized with a TCS-SP2 AOBS confocal laser-scanning microscope (Leica). For each embryo ≈40 sections of around 1 $\mu$m thickness were scanned along the *z* axis. The gain and offset were adjusted for each channel. Leica software was used to create an average snapshot of all sections for each embryo and images were processed in Photoshop (Adobe).

**Evaluation of the Posterior Expression Boundary.** For evaluation of posterior boundaries of endogenous gene expression in 0- to 3-h embryo collections, a custom made macro was used in ImageJ, which entailed drawing a rectangle around the entire embryo, to measure its length (X). The rectangle was kept fixed at the anterior pole of the embryo and shortened from the posterior to abut with the posteriormost point of expression (Y). The position of the posterior boundary in % egg length was calculated in Excel (Microsoft): $(100\% - (Y/X)) \times 100\% =$ position in %. The average and the standard deviation were calculated over the entire sample for each genotype.

Measurement of the posterior boundary of *lacZ* expression was also conducted in ImageJ using a slightly different protocol. Embryo cross-section pictures were collected and evaluated in a single-blind experiment. In the cross-section, a line was drawn through the embryo that followed the posterior boundary of *lacZ* expression. A second line was drawn through the entire length of the embryo, to assess its length (X) and the length of the line from the anterior tip to where it intersected with the line marking *lacZ* expression was taken as Y. The position of the posterior boundary in % egg length was calculated as stated above. The average and the standard deviation were calculated over the entire sample for each genotype.

**Assessment of Levels of Bcd Expression.** Bcd was detected with rat anti-Bcd (10) antibodies and Cy3 anti-rat antibodies from goat (Jackson ImmunoResearch). A cross-section of each embryo was captured using a TCS-SP2 AOBS confocal laser-scanning microscope (Leica) with an open pinhole. Gain and offset were kept constant between slides and genotypes. The 12-bit images

were then analyzed in ImageJ using a custom-made macro that subdivided the embryo into 20 equal parts and measured the brightness in each section. A background intensity was also measured for each image in an area of the picture devoid of sample. In Excel the background value for each image was subtracted from each intensity measured along the AP axis. The median intensity was evaluated for each embryo and the intensity measured at each point along the AP axis was divided by this median value to normalize the data. The normalized values were averaged for each point along the AP axis and the standard deviation was calculated.

***In silico* Screen for Potential torREs in Bcd Bound Genomic DNA Fragments.** To identify enhancers *in silico* that are likely to be regulated by Bcd and contain torREs, we focused on regions shown to be statistically significantly bound by Bcd in a chromatin immunoprecipitation assay followed by microarray analysis (11). We downloaded the coordinates of these regions (http://bdtnp.lbl.gov/Fly-Net/archives/chipper/Post_Processing/bcd_1_012505/bcd_1_012505-exp-1_table.txt) and retrieved the corresponding sequences.

To recapitulate the situation in the early embryo, we focused on the maternal factors involved in AP patterning at this time: Bcd, Caudal (Cad), Hunchback (Hb), and the presence of the torRE. The logic is that factors present at this time may compete for binding sites within the given Bcd-bound fragments. By screening these fragments for all four binding sites such potential competition is accounted for. We generated position weight matrices (PWMs) from the information provided by Schroeder et al. (3) for the maternal AP transcription factors Bcd, Hb, and Caudal. Furthermore, we also generated a PWM for the torRE, by using the eight 3′-most bases of the five known torso response elements, as these bases show high similarity with the preferred sequences of the human Cic homolog (12). The PWMs were generated by using all known binding sequences as seeds, which were "mutated" at each position by exchanging the correct base by either A, C, G, or T. Using all sequences, the frequency of bases at each position was determined. As background we simply determined the frequencies of the bases in the *Drosophila* genome (counting both the sense and anti-sense sequence, such that the frequency of A equals the frequency of T, as well as C equals G).

These PWMs and the background frequencies together with the sequences found to be bound by Bcd served as input to an algorithm that is essentially a modification of Ahab (3, 13). In the original version of Ahab, a conjugate gradient minimizer was used to minimize the negative log likelihood. We used the well-known Baum Welch algorithm (14) to find the maximum likelihood solution.

For each sequence we determined the log likelihood of the background alone ($\ln L_{back}$) and compared it to the likelihood obtained by adding the four PWMs ($\ln L_{full}$). To test whether the increase in likelihood found by adding the four PWMs is statistically significant, we used the log-likelihood ratio test for nested models (the model incorporating only the background is nested in the model with the four PWMs and the background). Because we added four PWMs there are four degrees of freedom. The log-likelihood ratio statistic $\Lambda = 2(\ln L_{full} - \ln L_{back})$ follows approximately a $\chi^2$ distribution with four degrees of freedom (15). The $P$ values are reported in Table S1.

For each of the sequences we determined the average number of binding sites for the four factors (13) and took the harmonic mean of the number of Bcd binding sites and the putative torREs as a score. The rationale for this kind of score was that we wanted to find enhancer sequences that have a high number of both torREs and Bcd binding sites. We took the top 50 regions and determined the neighboring genes.


1. Driever W, Nüsslein-Volhard C (1988) A gradient of *bicoid* protein in *Drosophila* embryos. *Cell* 54:83–93.
2. Macdonald PM, Struhl G (1988) *cis*-acting sequences responsible for anterior localization of *bicoid* mRNA in *Drosophila* embryos. *Nature* 336:595–598.
3. Schroeder MD, et al. (2004) Transcriptional control in the segmentation gene network of *Drosophila*. *PLoS Biol* 2:E271.
4. Mlodzik M, Fjose A, Gehring WJ (1988) Molecular structure and spatial expression of a homeobox gene from the *labial* region of the *Antennapedia*-complex. *EMBO J* 7:2569–2578.
5. Diederich RJ, Merrill VK, Pultz MA, Kaufman TC (1989) Isolation, structure, and expression of *labial*, a homeotic gene of the *Antennapedia* complex involved in *Drosophila* head development. *Genes Dev* 3:399–414.
6. Jiménez G, Guichet A, Ephrussi A, Casanova J (2000) Relief of gene repression by Torso RTK signaling: Role of *capicua* in *Drosophila* terminal and dorsoventral patterning. *Genes Dev* 14:224–231.
7. Ronchi E, Treisman J, Dostatni N, Struhl G, Desplan C (1993) Down-regulation of the *Drosophila* morphogen Bicoid by the Torso receptor-mediated signal transduction cascade. *Cell* 74:347–355.
8. Rørth P (1998) Gal4 in the *Drosophila* female germline. *Mech Dev* 78:113–118.
9. Liaw GJ, et al. (1995) The *torso* response element binds GAGA and NTF-1/Elf-1, and regulates *tailless* by relief of repression. *Genes Dev* 9:3163–3176.
10. Kosman D, Small S, Reinitz J (1998) Rapid preparation of a panel of polyclonal antibodies to *Drosophila* segmentation proteins. *Dev Genes Evol* 208:290–294.
11. Li XY, et al. (2008) Transcription factors bind thousands of active and inactive regions in the *Drosophila* blastoderm. *PLoS Biol* 6:27.
12. Kawamura-Saito M, et al. (2006) Fusion between CIC and DUX4 up-regulates PEA3 family genes in Ewing-like sarcomas with t(4;19)(q35;q13) translocation. *Hum Mol Genet* 15:2125–2137.
13. Rajewsky N, Vergassola M, Gaul U, Siggia ED (2002) Computational detection of genomic *cis*-regulatory modules applied to body patterning in the early *Drosophila* embryo. *BMC Bioinformatics* 3:30.
14. Durbin R (1998) *Biological Sequence Analysis: Probabilistic Models of Proteins and Nucleic Acids* (Cambridge Univ Press, Cambridge, UK) pp xi, 356.
15. Felsenstein J (1981) Evolutionary trees from DNA sequences: A maximum likelihood approach. *J Mol Evol* 17:368–376.

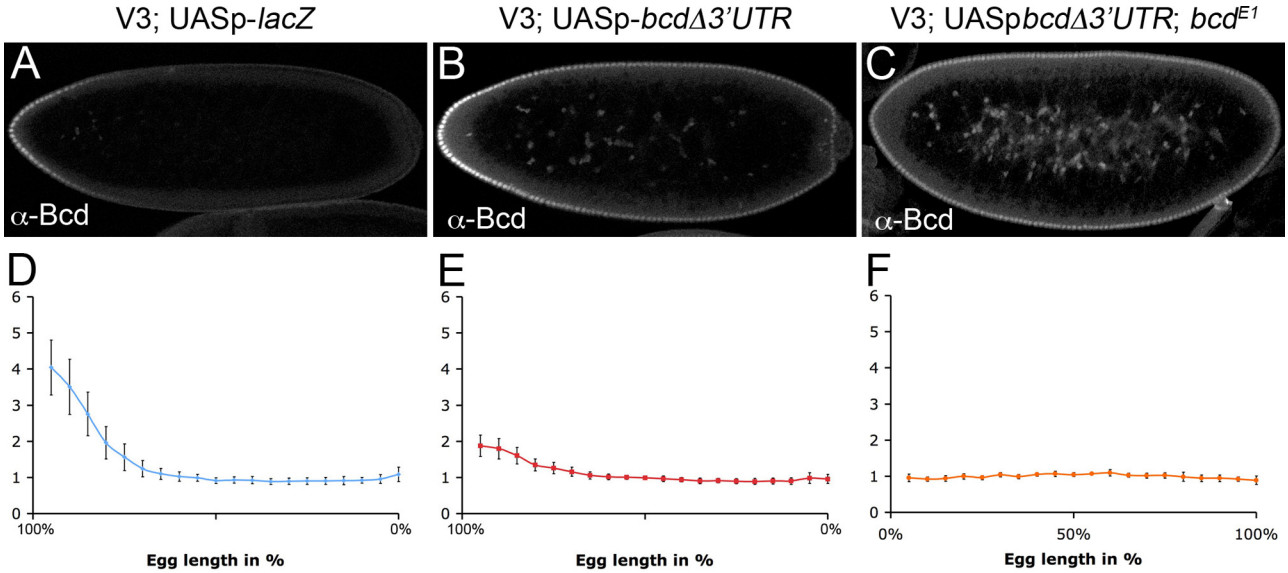


**Fig. S1.** Ectopic expression of Bcd in the female germline using the UASp/Gal4 system causes high levels of Bcd throughout the embryo. (*A*–*C*) Bcd was detected via fluorescent immunohistochemistry in control embryos, embryos ectopically expressing unlocalized Bcd and $bcd^{E1}$ embryos ectopically expressing unlocalized Bcd. Cross-sections are shown; anterior is to the *Left*. (*A*) In control embryos (V3) Bcd is detected in an AP gradient (1). (*B*) Expression of *bcd* lacking its localizing 3′-UTR (2) in the female germline results in ubiquitous Bcd. Higher levels of Bcd are detected in the anterior because of the endogenous Bcd present. (*C*) Ectopic expression of unlocalized Bcd results in uniform levels of Bcd throughout $bcd^{E1}$ embryos. (*D*–*F*) Assessment of Bcd expression along the anterior–posterior (AP) axis in control embryos, embryos ectopically expressing unlocalized Bcd and in $bcd^{E1}$ embryos ectopically expressing unlocalized Bcd. All embryos assessed were in stage 4. The fluorescent intensity was measured along the AP axis of individual embryos. To compare expression across samples, fluorescent intensity was normalized to the median intensity for each embryo. (*D*) An AP Bcd gradient is observed in the control embryos ($n = 17$). (*E*) A shallow AP gradient is also observed in embryos ectopically expressing unlocalized Bcd ($n = 12$), because of the endogenous Bcd present. Note however that no ectopic posterior to anterior gradient is detected. (*F*) No change in Bcd levels along the AP axis is detectable in $bcd^{E1}$ embryos ectopically expressing unlocalized Bcd ($n = 7$), indicating that in each embryo all nuclei are receiving the same amount of Bcd. *x* axis: egg length in %; anterior: 100%; posterior: 0%; *y* axis: normalized flourescent intensity; error bars: standard deviation.

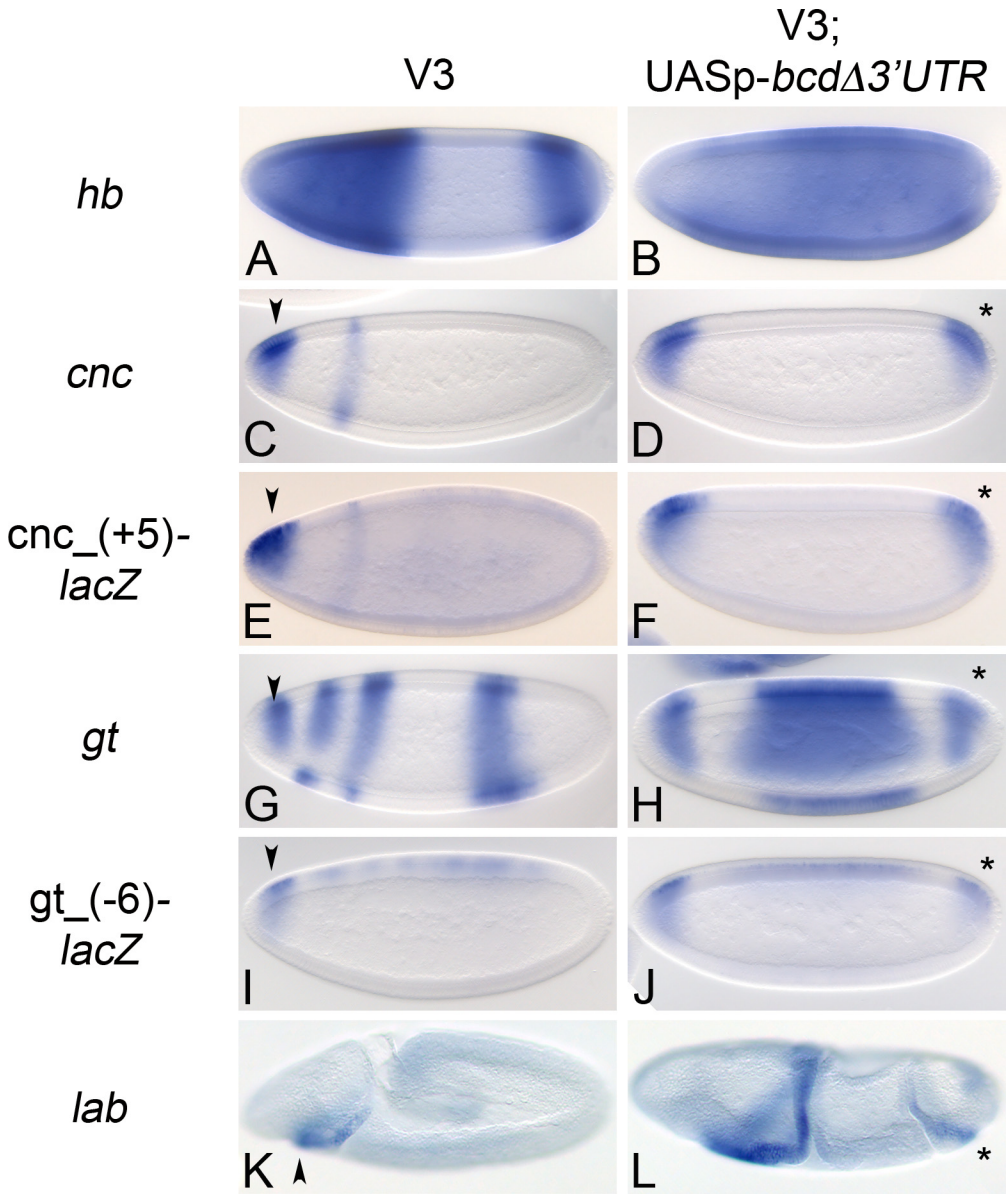


**Fig. S2.** Ectopic expression of unlocalized Bcd leads to mirror image duplications of anterior expression domains in the posterior by acting on known enhancer modules. Gene and *lacZ* expression was detected via *in situ* hybridization with the appropriate RNA anti-sense probes; anterior is to the *Left*; dorsal is *Up*. (*A*) In control embryos (V3 refers to V3-Gal4), *hb* is expressed in the anterior 50% of the embryo and in a posterior stripe. (*B*) Upon ectopic expression of unlocalized Bcd, *hb* is detected throughout the embryo, exempt only at the poles. (*C–J*) Unlocalized Bcd activates *cnc* and *gt* at the posterior through known enhancer modules. (*C*) *cnc* is expressed in an anterior cap domain (arrowhead) and a more posterior stripe in control embryos. (*D*) An ectopic cap domain is detected at the posterior pole (asterisk) in embryos ectopically expressing unlocalized Bcd. (*E*) cnc_(+5)-*lacZ* recapitulates *cnc* expression in control embryos (3). An anterior cap domain (arrowhead) and a more posterior stripe are observed. (*F*) Interestingly, *lacZ* expression is also detected in a posterior cap (asterisk) in embryos ectopically expressing unlocalized Bcd, similar to what is observed in *D*. (*G*) *gt* is expressed in an anterior tip domain (arrowhead), an anterior, discontinuous double stripe, and a posterior stripe in control embryos. (*H*) Upon the ectopic expression of unlocalized Bcd, *gt* is detected in an anterior and posterior tip domain (asterisk) and in a broad central domain. (*I*) gt_(−6)-*lacZ* recapitulates the expression of the *gt* anterior tip domain in control embryos (arrowhead) (3). (*J*) Ectopic *lacZ* expression is also detected at the posterior tip (asterisk) in embryos ectopically expressing unlocalized Bcd. The observations made with the cnc_(+5) and the gt_(−6)-*lacZ* constructs in the presence of unlocalized Bcd, indicate that ectopic Bcd is acting through enhancer modules, which are only active in the anterior in the wild-type situation and that the observed ectopic domains of *cnc* and *gt* indeed correspond to their anterior domains. (*K* and *L*) Uniform Bcd can cause the ectopic expression of the anterior *Hox* gene *labial* (*lab*) (4) in the posterior. (*K*) *lab* is expressed in a stripe of cells anterior to the cephalic furrow (4, 5) in control embryos (arrowhead). (*L*) In embryos expressing uniform levels of Bcd in the posterior, an ectopic stripe of *lab* is observed in some embryos (asterisk). Note that this stripe of expression lies posterior to a groove in the embryo, which could be equivalent to an ectopic cephalic furrow. As *Hox* genes define the identity of the cells in which they are expressed, we conclude that the ectopic expression of *lab* in these embryos indicates that the posterior has been transformed to take on anterior identity.

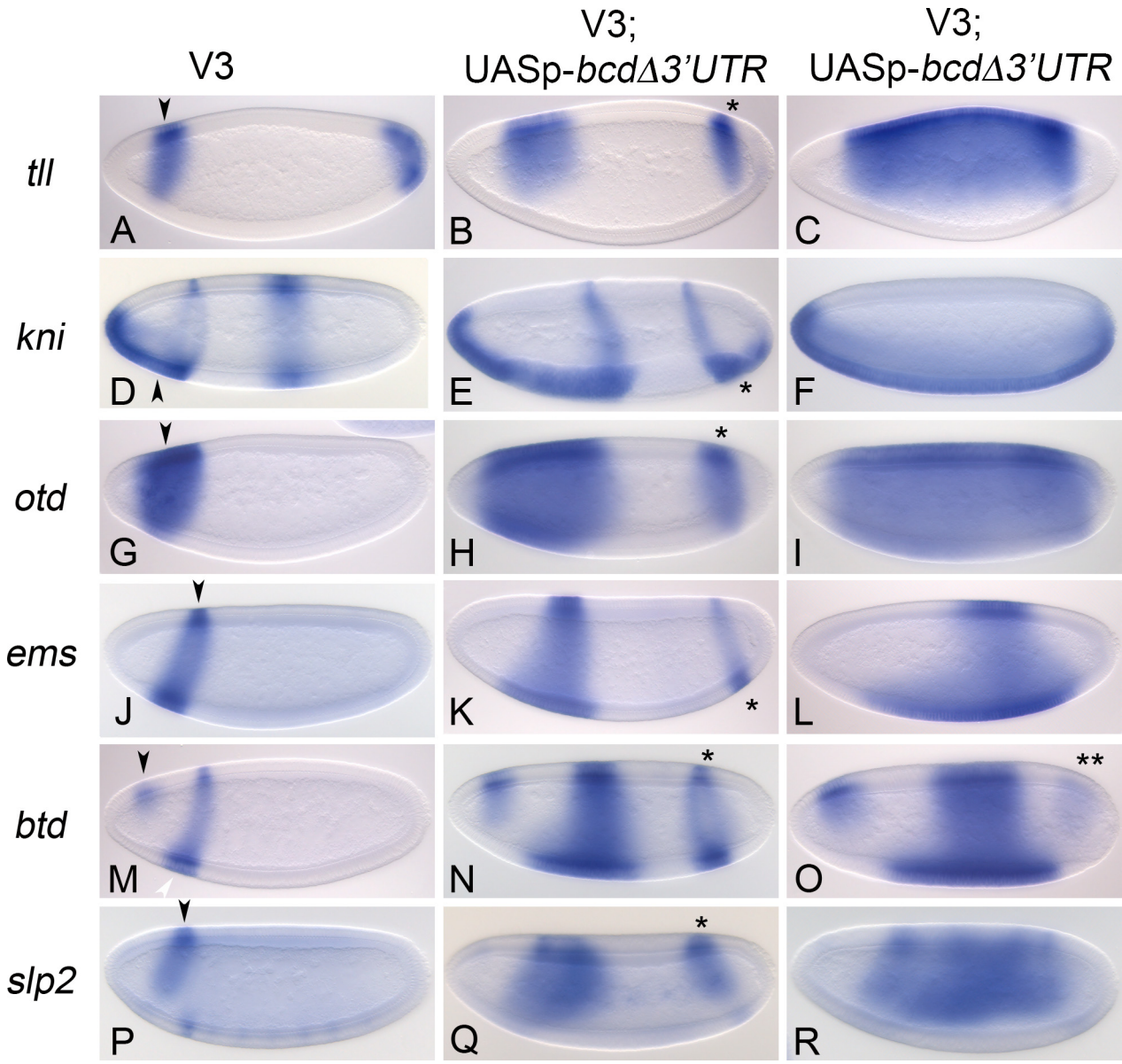


**Fig. S3.** Unlocalized Bcd leads to the mirror image duplication of anterior gene expression domains. Gene expression was detected by *in situ* hybridization using the appropriate RNA anti-sense probes. The *Left* column depicts control embryos (V3 refers to V3-Gal4), the *Middle* column depicts embryos ectopically expressing unlocalized Bcd exhibiting an intermediate phenotype, whereas the *Right* column depicts embryos ectopically expressing unlocalized Bcd exhibiting a strong phenotype; anterior is *Left*; dorsal is *Up*. (*A*) *tll* is expressed in an anterior dorsal-ventral wedge (arrowhead) and a posterior cap. (*B*) In embryos ectopically expressing unlocalized Bcd *tll* can be detected in an anterior and a posterior dorsal-ventral wedge (asterisk) or (*C*) in a central, ventrally repressed domain. (*D*) *kni* is detected in an anterior-ventral cap (arrowhead), an anterior stripe, and a posterior stripe. (*E*) In the presence of unlocalized Bcd, the anterior expression of *kni*, encompassing the ventral cap and the anterior stripe is duplicated with mirror image polarity in the posterior (asterisk). (*F*) A stronger effect of unlocalized Bcd is observed as continuous *kni* expression along the ventral side of the embryo. (*G*) *otd* expression is observed in a broad anterior stripe, which is repressed at the anterior tip (arrowhead) in control embryos. (*H*) In embryos ectopically expressing unlocalized Bcd, an ectopic posterior stripe of otd is observed (asterisk). (*I*) A stronger effect of unlocalized Bcd on *otd* is observed as expression throughout the embryo, exempt only from the poles. (*J*) *ems* expression is observed in an anterior stripe (arrowhead). (*K*) Ectopic expression of unlocalized Bcd leads to an ectopic stripe of *ems* in the posterior (asterisk) or (*L*) a central *ems* stripe. (*M*) *btd* is expressed in an anterior-dorsal ''button'' (black arrowhead) and a slightly more posterior stripe (white arrowhead). (*N*) Ectopic expression of unlocalized Bcd leads to the duplication of the stripe in the posterior (asterisk). (*O*) A stronger effect of unlocalized Bcd is observed as the duplication of the dorsal ''button'' domain in the posterior (double asterisk). (*P*) Early *slp2* expression is detected in the ventrally repressed stripe in the anterior in control embryos (arrowhead). (*Q*) In the presence of unlocalized Bcd *slp2* is also detected in a ventrally repressed stripe in the posterior (asterisk) or (*R*) in a broad central, ventrally repressed domain. Taken together, the observed gene expression patterns indicate that unlocalized Bcd causes the mirror image duplication of anterior gene expression domains in the posterior.

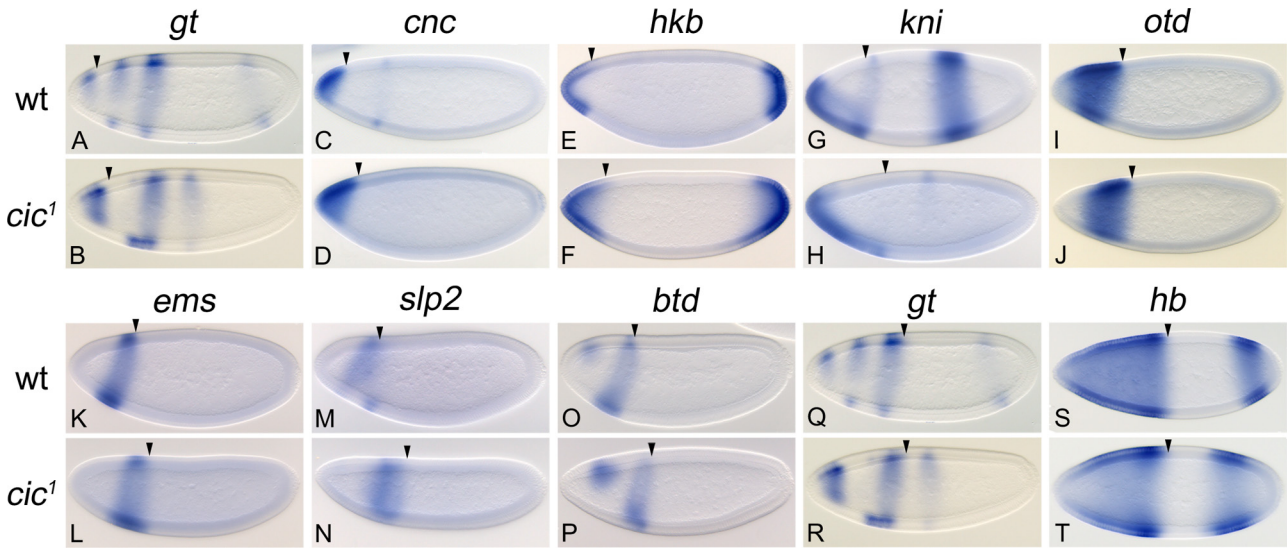


**Fig. S4.** Cic determines the position of the posterior boundary of Bcd target genes in the head. Bcd-dependent target genes were visualized with the appropriate RNA anti-sense probes by *in situ* hybridization in wild-type (wt) and *cic*$^{1}$ (6) embryos; anterior is to the Left, dorsal is *Up*; the arrowhead in each panel indicates the position of the posterior boundary (PB) summarized in Fig. 3*A*. (*A*) At the end of cellularization *gt* is expressed in an anterior tip domain, in an anterior stripe domain, consisting of a discontinuous and a continuous stripe, and in a posterior stripe domain. (*B*) In the absence of Cic, the PB of the *gt* tip domain is shifted toward the posterior (compare arrowhead in *B* to *A*). The posterior stripe is shifted toward the center, indicating that Cic also functions to limit the expression of posterior genes. This is most likely not Bcd dependent and not the subject of this work. (*C*) The expression of *cnc* is limited to an anterior cap and collar domain. (*D*) Whereas the collar domain is lost in *cic*$^{1}$ embryos, the PB of the cap domain is shifted toward the center (compare arrowhead in D to *C*). (*E*) *hkb* is expressed in an anterior and posterior cap in the blastoderm embryo. (*F*) The PB of the anterior domain is shifted toward the center in the absence of Cic (compare arrowhead in *E* to *F*). (*G*) *kni* is expressed in an anterior-ventral cap, an anterior stripe, and a posterior stripe. (*H*) In the absence of Cic the PB of the anterior-ventral domain is shifted toward the posterior, whereas the anterior stripe is not formed (compare position of arrowhead in *G* to *H*). (*I*) otd is expressed in a broad anterior domain, but is excluded from the anterior tip of the embryo. (*J*) The PB of *otd* expression is shifted to the posterior in the absence of Cic (compare position of arrowhead in *I* to *J*). (*K*) *ems* is expressed in an anterior stripe. (*L*) In the absence of Cic, the PB of *ems* expression is shifted to the posterior (compare arrowhead position in *K* and *L*). (*M*) *slp2* is expressed in an anterior, ventrally repressed stripe. (*N*) The PB of *slp2* is shifted to the posterior in *cic*$^{1}$ embryos (compare arrowhead position in *M* and *N*). (*O*) *btd* is expressed in an anterior-dorsal ''button'' and an anterior stripe. (*P*) In the absence of Cic, the PB of the *btd* stripe is shifted toward the posterior (compare arrowhead position in *O* and *P*). (*Q* and *R*) The same embryos are shown as in *A* and *B*, however, this time the position of the PB of the anterior stripe domain is of interest (arrowhead in *Q*). (*R*) In contrast to the PB of the anterior tip domain of *gt*, the PB of the anterior stripe domain is basically not shifted in the absence of Cic (compare arrowhead in *Q* to *R*). (*S*) In the embryo shown, *hb* is expressed in a broad domain, encompassing the anterior 50% of the embryo, and in a posterior stripe. (*T*) The PB of the anterior *hb* domain is not affected by the absence of Cic (compare arrowhead in *L* to *K*). Taken together, these results indicate that the effect of Cic is strongest on targets, with a PB of expression lying within the presumptive head region.

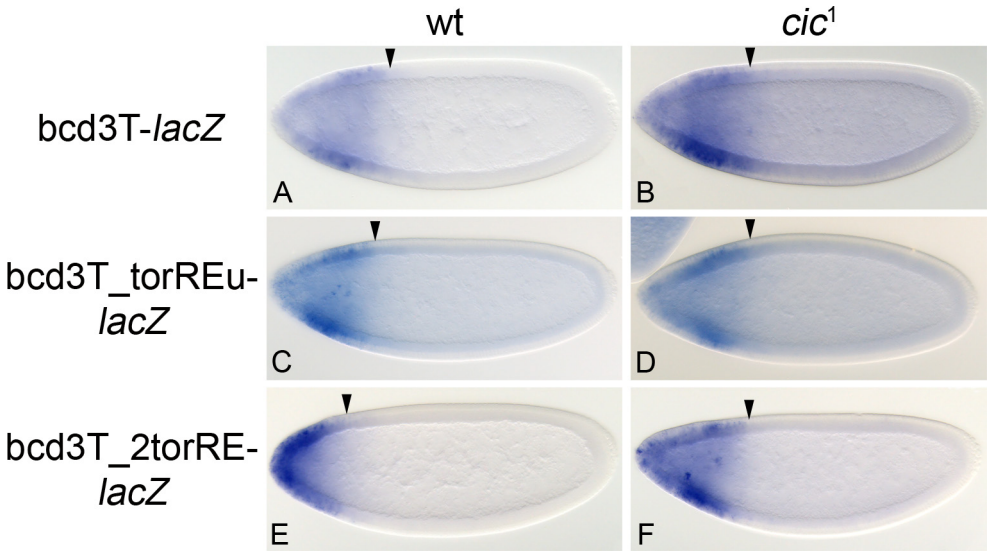


**Fig. S5.** Cic mediates repression through the torREs in a Bcd-dependent enhancer. The expression of *lacZ* mRNA was visualized by *in situ* hybridization in wild-type (wt) or *cic*$^{1}$ embryos carrying different *lacZ* reporters. The arrowhead in each panel indicates the position of the posterior boundary (PB) summarized in Fig. 3*C*; anterior is to the *Left*; dorsal is *Up*. (*A*) The bcd3T (7) construct drives *lacZ* expression in the anterior of wt embryos and is not influenced by the absence of Cic (*B*). (*C*) The bcd3T_1torREu activates *lacZ* expression in the anterior, but the PB of *lacZ* expression lies slightly more to the anterior than that of bcd3T-*lacZ*. Unlike the bcd3T, the bcd3T_1torREu is dependent on Cic (*D*). Addition of two torREs to the bcd3T has the strongest effect on *lacZ* expression (*E*). Note the anterior shift of *lacZ* expression when compared to bcd3T-*lacZ* (compare *E* to *A*). Like the bcd3T_1torREu the bcd3T_2torRE is dependent on the presence of Cic (*F*). The PB of *lacZ* driven by bcd3T_1torREu and bcd3T_2torRE in *cic*$^{1}$ embryos is located at approximately the same position as the PB of *lacZ* expression under bcd3T control. These results indicate that the torREs mediate repressive effects of Cic in Bcd-responsive enhancers and that Cic does not have a direct negative effect on Bcd.

**Table S1. Bcd-bound genomic fragments contain torREs**

| Genome coordinate | Bound region score | Length, bp | Bcd | Hb | Cad | torRE | Score | Flanking targets 1 | Flanking targets 2 | Known enhancer | *P* value |
|---|---|---|---|---|---|---|---|---|---|---|---|
| Chr 3R 26,674,402–26,678,742 | 2.35 | 4,341 | **31.04** | 28.81 | 16.39 | 18.11 | 23.71 | CG15544 | tll | tll_P2, tll_P3, tll_K2 | 1.96*E*-30 |
| Chr 3L: 4,674,848–4,679,178 | 2.35 | 4,331 | **28.07** | 25.23 | 22.50 | 19.08 | 23.14 | CG15876 | CG13713 | — | 1.24*E*-23 |
| Chr 2R: 9,076,518–9,081,137 | 1.71 | 4,620 | **24.92** | 32.13 | 22.53 | 13.36 | 18.24 | CG13334 | CG13335 | — | 1.19*E*-19 |
| Chr 2R: 16,468,154–16,470,997 | 1.89 | 2,844 | **17.29** | 10.98 | 3.28 | 14.28 | 15.71 | hbn | CG15649 | — | 8.08*E*-10 |
| Chr 3R: 9,703,419–9,706,393 | 1.82 | 2,975 | **36.06** | 22.51 | 3.40 | 6.70 | 15.55 | E5 | ems | — | 1.52*E*-14 |
| Chr X: 8,498,506–8,500,970 | 1.80 | 2,465 | **27.81** | 17.86 | 0.01 | 7.80 | 14.72 | otd | CG12772 | otd_early | 1.70*E*-11 |
| Chr X: 2,289,681–2,291,818 | 1.55 | 2,138 | **29.62** | 14.87 | 0.01 | 6.92 | 14.32 | gt | tko | gt_(−6) | 3.64*E*-14 |
| Chr 3L: 20,632,626–20,634,810 | 1.84 | 2,185 | **21.61** | 28.44 | 0.02 | 9.44 | 14.28 | kni | CG13253 | kni_(−5) | 1.21*E*-15 |
| Chr 2R: 3,743,615–3,746,471 | 1.37 | 2,857 | **25.35** | 20.57 | 6.94 | 7.93 | 14.18 | dpn | pnut | — | 5.44*E*-12 |
| Chr 2L: 13,224,097–13,228,532 | 2.43 | 4,436 | **20.97** | 30.41 | 3.85 | 9.38 | 14.02 | CG15480 | CG16813 | — | 2.59*E*-09 |
| Chr 2L: 12,080,452–12,082,438 | 2.38 | 1,987 | **27.32** | 19.70 | 0.43 | 6.24 | 13.05 | CG14947 | prd | — | 9.39*E*-11 |
| Chr 2L: 2,163,997–2,165,941 | 1.36 | 1,945 | **11.86** | 17.16 | 0.03 | 13.58 | 12.69 | CG7263 | aop | — | 4.83*E*-07 |
| Chr 2L: 3,832,748–3,835,221 | 2.64 | 2,474 | **23.56** | 25.00 | 3.87 | 6.30 | 12.18 | slp1 | slp2 | slp2_(−3) | 4.76*E*-14 |
| Chr 3R: 26,680,529–26,683,416 | 2.03 | 2,888 | **37.51** | 25.91 | 4.30 | 3.61 | 11.64 | tll | CG12045 | — | 1.64*E*-14 |
| Chr 2R: 20,729,106–20,733,256 | 2.72 | 4,151 | **39.48** | 79.84 | 19.38 | 3.38 | 11.54 | CG9380 | Kr | Kr_CD2_AD1 Kr_CD1 | 4.34*E*-53 |
| Chr 2L: 1,957,006–1,959,082 | 1.66 | 2,077 | **25.28** | 11.16 | 0.04 | 4.65 | 10.84 | CG31670 | CG10908 | — | 7.82*E*-08 |
| Chr 3R: 19,020,548–19,022,358 | 1.41 | 1,811 | **14.15** | 23.32 | 2.75 | 8.28 | 10.83 | cnc | fzo | cnc_(+5) | 2.00*E*-15 |
| Chr 2R: 7,309,605–7,312,008 | 1.58 | 2,404 | **9.43** | 28.50 | 1.21 | 11.50 | 10.42 | ths | Tango3 | — | 1.53*E*-13 |
| Chr 3R: 4,523,824–4,527,324 | 3.19 | 3,501 | **29.46** | 46.07 | 6.96 | 3.46 | 10.09 | hb | CG8112 | hb_central stripe and posterior | 2.66*E*-27 |
| Chr 2R: 18,713,564–18,715,511 | 1.13 | 1,948 | **18.71** | 23.12 | 3.51 | 5.31 | 9.97 | CG34371 | CG3162 | — | 6.41*E*-12 |
| Chr 3L: 14,114,265–14,117,624 | 2.00 | 3,360 | **9.61** | 40.84 | 16.75 | 10.14 | 9.87 | Sox21b | D | — | 8.04*E*-19 |
| Chr X: 9,534,773–9,537,554 | 1.80 | 2,782 | **26.94** | 18.67 | 5.78 | 3.62 | 9.87 | CG15321 | btd | btd_head | 3.28*E*-13 |
| Chr 2L: 6,372,450–6,377,368 | 1.36 | 4,919 | **27.92** | 4.98 | 1.18 | 3.41 | 9.75 | slam | CG13981 | — | 7.41*E*-03 |
| Chr X: 18,137,106–18,139,443 | 2.30 | 2,338 | **20.36** | 26.77 | 1.11 | 4.53 | 9.60 | CG15061 | os | — | 1.39*E*-15 |
| Chr X: 438,918–441,667 | 0.85 | 2,750 | **12.38** | 21.90 | 5.93 | 7.05 | 9.34 | App1 | vnd | — | 1.02*E*-10 |
| Chr 2R: 3,640,836–3,642,265 | 1.21 | 1,430 | **18.77** | 1.41 | 1.44 | 4.62 | 9.32 | Socs44A | CG11508 | — | 7.21*E*-05 |
| Chr 3R: 15,756,114–15,757,779 | 0.98 | 1,666 | **12.81** | 15.82 | 15.71 | 6.51 | 9.13 | Hs6 st | mira | — | 3.02*E*-14 |
| Chr 2R: 14,787,225–14,789,284 | 1.98 | 2,060 | **10.12** | 40.27 | 0.09 | 8.18 | 9.10 | CG7229 | rib | — | 6.78*E*-22 |
| Chr 2L: 13,866,970–13,869,110 | 1.53 | 2,141 | **10.54** | 11.26 | 0.88 | 7.83 | 9.08 | CG7968 | cenG1A | — | 3.74*E*-06 |
| Chr 3R: 11,408,184–11,410,171 | 1.60 | 1,988 | **18.98** | 10.40 | 2.31 | 4.32 | 9.05 | CG18516 | CG5302 | — | 6.34*E*-06 |
| Chr X: 20,501,020–20,504,083 | 1.52 | 3,064 | **33.79** | 18.06 | 15.10 | 2.32 | 8.86 | hydra | run | run_7_stripe | 5.22*E*-20 |
| Chr 3L: 3,495,119–3,496,376 | 0.97 | 1,258 | **16.02** | 0.00 | 5.04 | 4.88 | 8.84 | CG14973 | ImpE2 | — | 4.32*E*-05 |
| Chr 2L: 599,853–602,474 | 1.77 | 2,622 | **17.48** | 30.42 | 0.35 | 4.47 | 8.84 | Gsc | CG13689 | — | 5.24*E*-12 |
| Chr 2L: 12,723,437–12,724,872 | 0.92 | 1,436 | **16.39** | 2.63 | 0.00 | 4.61 | 8.69 | CG5792 | CG6214 | — | 1.35*E*-04 |
| Chr X: 11,166,778–11,169,127 | 1.89 | 2,350 | **23.81** | 9.42 | 0.48 | 3.17 | 8.68 | sisA | l(1)10Bb | — | 5.62*E*-07 |
| Chr 3R: 19,705,212–19,706,839 | 1.16 | 1,628 | **12.68** | 29.26 | 0.01 | 5.91 | 8.65 | CG12492 | Pli | — | 6.89*E*-12 |
| Chr 3R: 25,866,086–25,868,507 | 1.63 | 2,422 | **15.36** | 0.00 | 0.00 | 4.86 | 8.64 | Sry-beta | Sry-alpha | — | 2.88*E*-03 |
| Chr 3R: 13,905,810–13,907,959 | 1.61 | 2,150 | **16.39** | 6.49 | 1.29 | 4.53 | 8.62 | htl | CG14317 | — | 2.03*E*-03 |
| Chr 3R: 21,457,912–21,460,117 | 1.51 | 2,206 | **18.54** | 33.44 | 4.14 | 3.95 | 8.56 | CG4685 | jigri | — | 3.96*E*-18 |
| Chr 2L: 12,662,433–12,663,546 | 0.85 | 1,114 | **8.68** | 4.08 | 4.52 | 8.13 | 8.40 | pdm2 | CG15485 | — | 2.37*E*-04 |
| Chr 2L: 18,592,537–18,595,618 | 1.73 | 3,082 | **13.01** | 20.63 | 0.14 | 5.41 | 8.39 | amos | CG10413 | — | 2.22*E*-07 |
| Chr X: 6,889,156–6,890,844 | 1.40 | 1,689 | **16.86** | 11.54 | 0.85 | 4.15 | 8.36 | CG14427 | nullo | — | 2.45*E*-09 |
| Chr 3R: 19,974,704–19,976,154 | 1.12 | 1,451 | **12.95** | 12.79 | 2.58 | 5.25 | 8.25 | CG31133 | p38c | — | 2.66*E*-05 |
| Chr X: 255,967–257,414 | 1.31 | 1,448 | **14.58** | 17.54 | 6.70 | 4.66 | 8.24 | sc | l(1)sc | — | 5.57*E*-09 |
| Chr X: 20,490,149–20,492,000 | 1.80 | 1,852 | **11.17** | 9.15 | 1.86 | 6.08 | 8.24 | hydra | run | run_stripe7 run_stripe1 | 1.63*E*-03 |
| Chr X: 3,253,337–3,254,712 | 0.99 | 1,376 | **10.08** | 11.17 | 0.01 | 6.64 | 8.18 | dm | CG12535 | — | 1.70*E*-07 |
| Chr 2R: 7,029,859–7,030,732 | 0.67 | 874 | **14.03** | 0.05 | 2.91 | 4.71 | 8.13 | inv | CG30034 | — | 8.27*E*-05 |
| Chr 3R: 2,579,058–2,581,883 | 1.27 | 2,826 | **20.23** | 15.53 | 7.66 | 3.05 | 7.85 | zen | CG1162 | — | 8.78*E*-07 |
| Chr 3R: 679,356–681,178 | 1.43 | 1,823 | **16.79** | 3.08 | 5.44 | 3.65 | 7.83 | opa | laf | — | 3.36*E*-05 |
| Chr 2R: 6,752,839–6,754,422 | 1.48 | 1,584 | **13.22** | 4.20 | 6.47 | 4.53 | 7.74 | CG34224 | CG13216 | — | 9.53*E*-04 |

Bcd-bound fragments obtained (1) were assessed for the presence of torREs and the binding sites for the maternal AP transcription factors Bcd, Caudal (Cad), and Hunchback (Hb) by using a modified version of the Ahab algorithm (2) (see *SI Materials and Methods*). The average number of Bcd (boldface), Cad, and Hb binding sites and torREs (underlined) are shown for a given fragment length. Fragments were scored for a high number of both torREs and Bcd binding sites. Note that some fragments overlap known enhancer modules that were shown to be active in the head region, [e.g., gt_(−6), kni_(−5), and *cnc*_(+5); see ref. 3 and references therein]; others are located in the vicinity of potential Bcd target genes in the head region [e.g., *empty spiracles* (*ems*), *homeobrain* (*hbn*), *goosecoid* (*gsc*), and *Dicheate* (*D*)] or genes of unknown function such as *CG31670* that have anterior expression domains. Genome coordinate is based on the *Drosophila melanogaster* genome release 4.0. For bound region score, see ref. 1. Score, harmonic mean of the average number of Bcd sites and the average number of torREs; known enhancers, according to ref. 3; *P* value, calculated using the $\chi^2$ statistic of the log-likelihood ratio test for nested models with four degrees of freedom (see *SI Materials and Methods*).


1. Li XY, et al. (2008) Transcription factors bind thousands of active and inactive regions in the *Drosophila* blastoderm. *PLoS Biol* 6:e27.
2. Rajewsky N, Vergassola M, Gaul U, Siggia ED (2002) Computational detection of genomic *cis*-regulatory modules applied to body patterning in the early *Drosophila* embryo. *BMC Bioinformatics* 3:30.
3. Schroeder MD, et al. (2004) Transcriptional control in the segmentation gene network of *Drosophila*. *PLoS Biol* 2:E271.